Molecular-alignment dependence of collision-induced dissociation and electron capture in $H_2^+ + He$ collisions

C. H. Liu,[1] J. G. Wang,[2] and R. K. Janev[3,4]

[1]*Institute of Modern Physics, Chinese Academy of Sciences, Lanzhou 730000, People's Republic of China*

[2]*Data Center for High Energy Density Matter, Institute of Applied Physics and Computational Mathematics, P. O. Box 8009, Beijing 100088, People's Republic of China*

[3]*Macedonian Academy of Sciences and Arts, P. O. Box 428, 1000 Skopje, Macedonia*

[4]*Institute of Energy and Climate Research–Plasma Physics, Forschungszentrum Jülich GmbH, Association EURATOM-FZJ, Trilateral Euregio Cluster, 52425 Jülich, Germany*

(Received 13 April 2014; published 27 June 2014)

The collision-induced dissociation (CID), electron capture (EC), and dissociative capture (DC) processes in $H_2^+ + He$ collision are investigated by the quantum-mechanical molecular-orbital close-coupling method in the energy range of 0.02–10 keV/u. The studies are based on the *ab initio* calculation of the molecular structure data for different H_2^+ alignments with respect to the incident beam direction. The cross sections are compared with the available experimental and theoretical results. The CID process dominates the EC and DC processes. The CID cross sections sensitively depend on the molecular orientations at the time of dissociation in the energy region considered. Dissociation is found to be more likely to occur when the molecular axis is aligned perpendicular to the collision trajectory. The rotational couplings play an important role in dissociation processes.

DOI: 10.1103/PhysRevA.89.062719 PACS number(s): 34.70.+e, 34.20.−b

I. INTRODUCTION

Collisions of molecular ions with atoms are recognized as fundamental processes in astrophysics, Earth's ionosphere, and in many industrial plasmas. In such collisions, various reactions can take place, including dissociation, electron capture, excitation, ionization, and so on. Being among the simplest multielectron ion-molecule collision systems, the H_2^+-He collision system has been rather extensively experimentally studied in the past, with particular attention being paid to the collision-induced dissociation (CID) [1-3], electron capture (EC) [3], dissociative capture (DC) [3], emission of radiation [4,5], and target excitation [6]. Fedorenko *et al*. [1] measured the total proton-production cross sections for H_2^+ colliding with He target at 5–300 keV. The dissociation of 2–50 keV H_2^+ ions into H^+ and H ions has been measured in inert-gas targets by Williams and Dunbar [2] through detecting the ion formation. Suzuki *et al.* [3] measured the dissociated fragments, neutral particles, and ionized target atoms resulting from the collisions of H_2^+ ions with He, Ne, and Ar atoms in the projectile energy range of 4–16 keV. The cross sections of EC and CID with and without target ionization are derived in this work by solving a set of the rate equations. Their experiment for $H_2^+ + He$ collision shows that the CID cross sections are larger than those of the EC and DC processes, and slowly increase with decreasing of energy. This energy dependence is different than that observed by Fedorenko *et al*. [1] and Williams and Dunbar [2], in which the H^+ formation cross sections decrease monotonously with decreasing energy. At energies below 1 keV/u, no experimental results are available for integral cross sections.

From a theoretical point of view, since one of the collision partners is a molecular ion, the study of the $H_2^+ + He$ collision system is much more complex than the atomic ion-atom systems due to the increase in the degrees of freedom and due to the more complex collision geometry. Consequently, the number of reaction channels can increase significantly and the coupling of angular momenta becomes more complex. The latter fact makes it necessary to use various decoupling approximations to make the calculations tractable [7,8]. For the H_2^+-He collision, more systematic theoretical research needs to be carried out for energies below 1 keV/u, and very limited theoretical studies have been performed in the intermediate- and high-energy region. Green and Peek [9] performed the Born approximation calculations for the breakup of H_2^+ ions colliding with He for energies above 20 keV. In the few-keV energy region, Furlan and Russek [10] have investigated the EC, CID, and excitation processes using the straight-line trajectory method based on the *ab initio* molecular structure. In their calculations, however, only the lowest three molecular states were included. Their CID cross sections are several times smaller than the experimental results of Refs. [2,3], and the EC results are about one order larger than the measurements of Ref. [3].

In the present work we shall study the CID, EC, and DC processes in the $H_2^+ + He$ collision for different alignments of the incident molecular ion using the quantum-mechanical molecular-orbital close-coupling (QMOCC) methods [11,12] in the energy range of 0.02–10 keV/u. The vibrational and rotational motions of the molecular ion were neglected. The *ab initio* molecular structure was calculated by the multireference single- and double-excitation configuration interaction (MRDCI) method [13,14]. With the calculated molecular structure data, we were able to include in our QMOCC calculation the following reaction channels (see Fig. 1):

$$\begin{aligned} H_2^+(1s\sigma_g) + He(1s^2) &\rightarrow H_2(1s\,^1\Sigma_g) + He^+(1s) \quad \text{(a)} \\ &\rightarrow H_2^+(2p\sigma_u) + He(1s^2) \quad \text{(b)} \\ &\rightarrow H_2(2p^3\Sigma_u) + He^+(1s) \quad \text{(c)} \\ &\rightarrow H_2^+(2p\pi_u) + He(1s^2) \quad \text{(d)} \\ &\rightarrow H_2^+(1s\sigma_g) + He(1s2s) \quad \text{(e)}\,. \end{aligned} \tag{1}$$

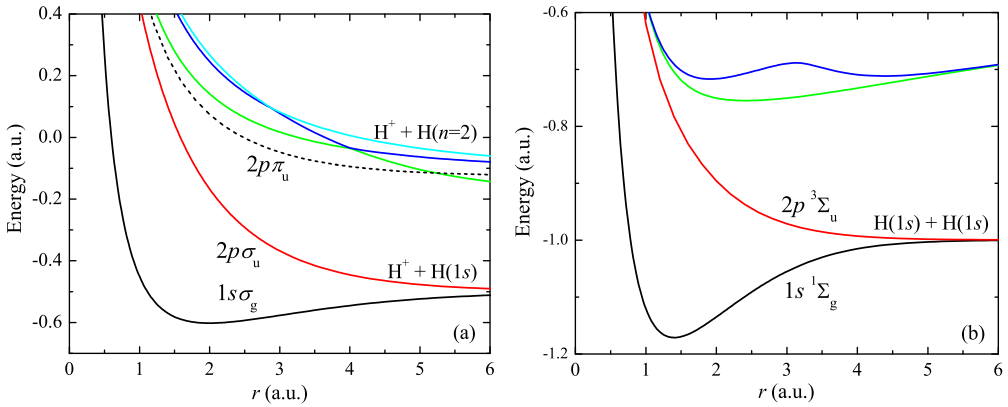

FIG. 1. (Color online) Potential energy curves for (a) H_2^+ and (b) H_2.

The reaction channel (a) represents the EC process, reaction channels (b) and (d) contribute to the CID process, reaction channel (c) represents the DC process, and channel (e) is excitation of He to its metastable $2s$ state.

The paper is organized as follows. In the next section we briefly outline the theoretical methods used in the present study. In Sec. III we present the *ab initio* molecular structure data calculated by the MRDCI method. In Sec. IV we show the calculated cross sections for the CID, EC, and DC processes in the energy range 0.02–10 keV/u. In Sec. V we give our conclusions.

Atomic units will be used throughout unless explicitly indicated otherwise.

II. THEORETICAL METHODS

The QMOCC method in ion-atom collisions has been described thoroughly in the literature [11,12]. For a collision system involving diatomic molecules, the sudden approximation [7,8,15] is introduced for the rotational and vibrational motion of the diatom. In other words, at nuclear velocities that are sufficiently large, the diatomic molecule can be considered to have fixed orientation and geometry during the excitation process. Then the cross sections can be calculated in the same way as in ion-atom collisions. The QMOCC method involves solution of a coupled set of second-order differential equations using the log-derivative method of Johnson [16]. In the adiabatic representation, transitions between channels are driven by radial and rotational (A^r and A^θ) couplings of the vector potential $\mathbf{A}(\mathbf{R})$, where $\mathbf{R}$ is the internuclear distance vector. The allowance for the translation effects is made by adding the quadrupole moment tensor terms into the radial and rotational coupling matrix elements according to Ref. [17].

The coupled set of second-order differential equations is solved and matched to the plane-wave boundary conditions at a large internuclear distance, $R_{\max}$, to obtain the K matrix. Then the scattering matrix S is given by

$$S_J = [I + iK_J]^{-1}[I - iK_J], \tag{2}$$

where I is the identity matrix and J is the total angular momentum quantum number. Finally, the cross section for transition from channel α to channel β is expressed in terms of scattering matrix elements,

$$\sigma_{\alpha\to\beta} = \frac{\pi}{k_\alpha^2}\sum_J (2J+1)|\delta_{\alpha\beta} - S^J_{\alpha\beta}|^2, \tag{3}$$

where k_α denotes the initial momentum of center-of-mass motion.

III. MOLECULAR STRUCTURE CALCULATIONS

The MRDCI method [13,14] was employed to calculate the molecular data (potential energy curves, and radial and rotational coupling matrix elements) of the considered collision system. In the molecular structure calculations, the correlation-consistent, polarization valence, triple-ζ-(cc-pVTZ)-type basis set [18] with a diffuse $(2s2p)$ basis was used for the H atom. The cc-pVTZ-type basis set [18] with a diffuse $(2s2p2d)$ basis was employed for the He atom. The final contracted basis set for the hydrogen atom was $(7s, 4p, 1d)/[5s, 4p, 1d]$ and for the He atom it was $(8s, 4p, 3d)/[5s, 4p, 3d]$. Firstly, using the same basis set, we calculated the potential curves for the H_2 and H_2^+ molecules as shown in Fig. 1. From the potentials of H_2^+ we know that the $2p\sigma_u$ state is repulsive, and the $2p\pi_u$ state is very weakly bound with an equilibrium bond length greatly larger than that of the $H_2^+(1s\sigma_g)$ ground state. If these excited states are formed by vertical Franck-Condon transitions, the H_2^+ molecular ion would immediately dissociate. The $H_2(2p\ ^3\Sigma_u)$ state is also repulsive. As mentioned earlier and evident from Fig. 1, the channel (a) represents the EC process, the channels (b) and (d) represent the CID process, and the channel (c) represents the DC process, while the channel (e) represents excitation of the He target.

The diatomic ion-atom scattering differs from the atomic ion-atom scattering by the presence of alignment-dependent interactions. In the present calculations for the $H_2^+ + He$ collision system, the geometry was defined (see Fig. 2) by the H-H internuclear vector, $\mathbf{r}$, the internuclear radius vector from the center of the H-H bond to the nucleus of the He atom, $\mathbf{R}$, and the angle θ between them. The calculations were carried out for the H-H separation of $r = 2.0$ a.u., which is the equilibrium bond length of the $H_2^+(1s\sigma_g)$ ground state and is valid to describe the collisions of H_2^+ and He. The angular variable θ was chosen to be 0, $\pi/4$, and $\pi/2$. For $\theta = 0$ and $\pi/2$, the molecular geometry has C_{2v} symmetry, while for the other orientations, the system's geometry is described by C_s symmetry.

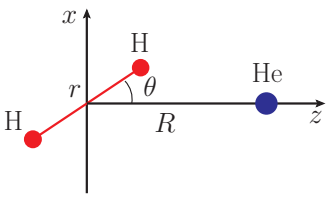

FIG. 2. (Color online) The molecular geometry.

The potential energy curves for the low-lying molecular states of HeH_2^+ ion, calculated in the present work, are shown in Figs. 3(a)–3(c) for $\theta = 0$, $\pi/4$, and $\pi/2$, respectively. The 1^2A_1 states for $\theta = 0$ and $\pi/2$ and the $1^2A'$ state for $\theta = \pi/4$ represent the initial channels for the $H_2^+(1s\sigma_g) + He$ collision. It should be noted that the states asymptotically corresponding to the $H_2^+(2p\sigma_u) + He(1s^2)$ and $H_2(2p\ ^3\Sigma_u) + He^+(1s)$ configurations have an A_1 symmetry for $\theta = 0$, but acquire a B_2 symmetry for $\theta = \pi/2$ according to the alignment of these molecular states with respect to the collision vector **R**. The opposite becomes true for the $H_2^+(2p\pi_u) + He(1s^2)$ state. For other orientations, these configurations have both the parallel and perpendicular projections with respect to **R**, which represent the Σ and Π components, respectively. We note that for $\theta = 0$, because the B_1 and B_2 states have the same potential curves, only the A_1 and B_1 states are included in the QMOCC calculation. For $\theta = \pi/2$, because the B_1 and B_2 states are no longer symmetric, all of the A_1, B_1, and B_2 states should be included in the basis. For $\theta = \pi/4$, the A' and A'' states should be included in the calculations.

In Fig. 4 we show some important radial coupling matrix elements. It is evident that the positions of the peaks in radial couplings are consistent with the avoided crossings of the adiabatic potentials. The weak radial couplings 1^2A_1-2^2A_1 and $1^2A_1 - 3^2A_1$ (or $1^2A'$ -$2^2A'$ and $1^2A' - 3^2A'$), which are mainly responsible for EC and CID processes, are plotted by a magnification factor of 10 to make it easier to see. Except for $\theta = \pi/2$, there are strong radial couplings between $2^2A'$ and $3^2A'$ states (or 2^2A_1 and 3^2A_1 states for $\theta = 0$) at about 3 a.u. These couplings are responsible for the rearrangement of the system between the EC and CID processes. At internuclear distances larger than about 3.5 a.u., the $2^2A'$ state (or 2^2A_1 state for $\theta = 0$) denotes the $H_2(1s\ ^1\Sigma_g) + He^+$ configuration and the $3^2A'$ state (or 3^2A_1 state for $\theta = 0$) denotes the $H_2^+(2p\sigma_u) + He$ configuration, but at smaller R, the $2^2A'$, $3^2A'$ states exert an avoided crossing at about $R_x \approx 3.15$ a.u. ($R_x \approx 3.33$ a.u. for the 2^2A_1, $3\ ^2A_1$ states at $\theta = 0$) resulting in exchange of the configurations. For $\theta = \pi/2$, because the states that asymptotically relate to the $H_2^+(2p\sigma_u) + He$ and $H_2(2p\ ^3\Sigma_u) + He^+$ configurations become B_2 states (see Fig. 3), the system cannot be directly excited to these states by radial couplings. For all collision angles, there exist series of radial couplings between the $H_2 + He^+$ configurations with the upper H_2^+-He configurations (see series of radial couplings in the

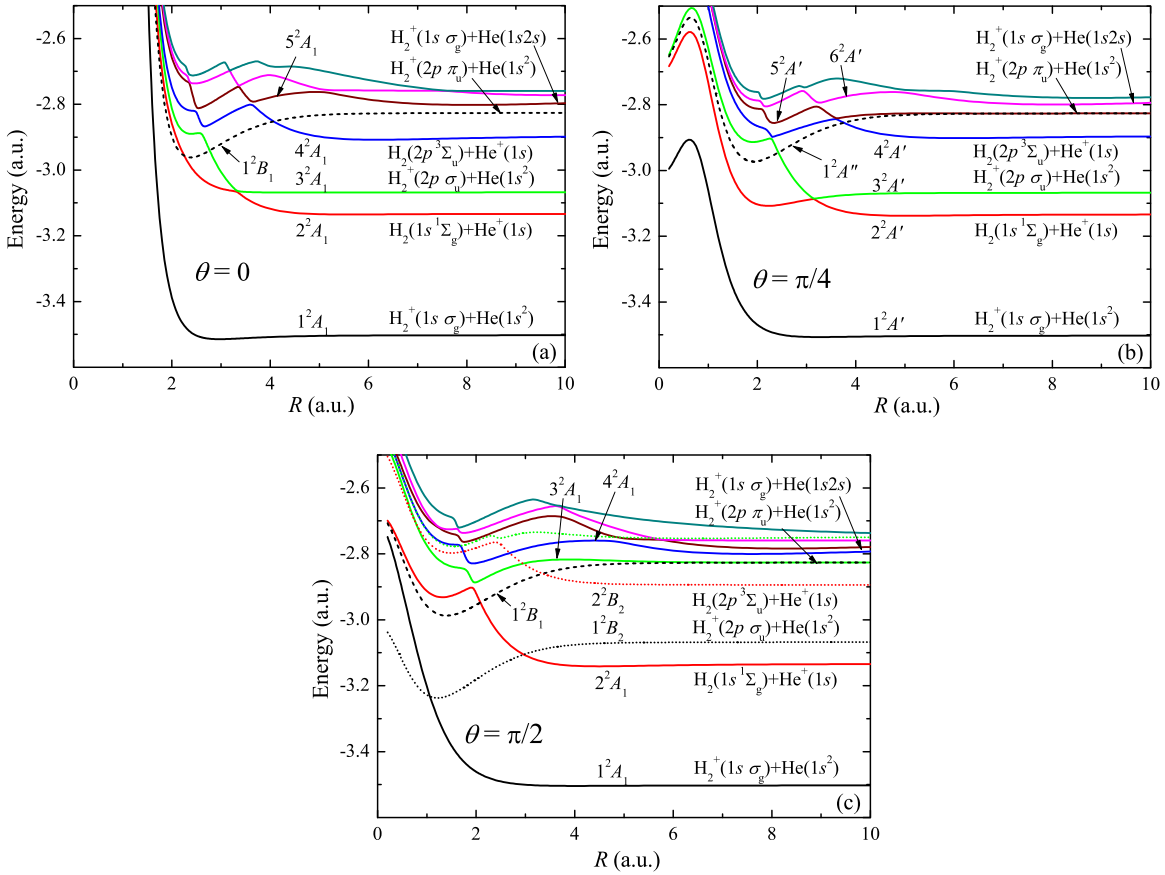

FIG. 3. (Color online) Potential energy curves for HeH_2^+. (a) $\theta = 0$; (b) $\theta = \pi/4$; (c) $\theta = \pi/2$. The solid, dashed, and dotted lines represent the $^2A_1$, $^2B_1$, and $^2B_2$ states for $\theta = 0$ and $\pi/2$, and the solid and dashed lines represent the $^2A'$ and $^2A''$ states for $\theta = \pi/4$, respectively.

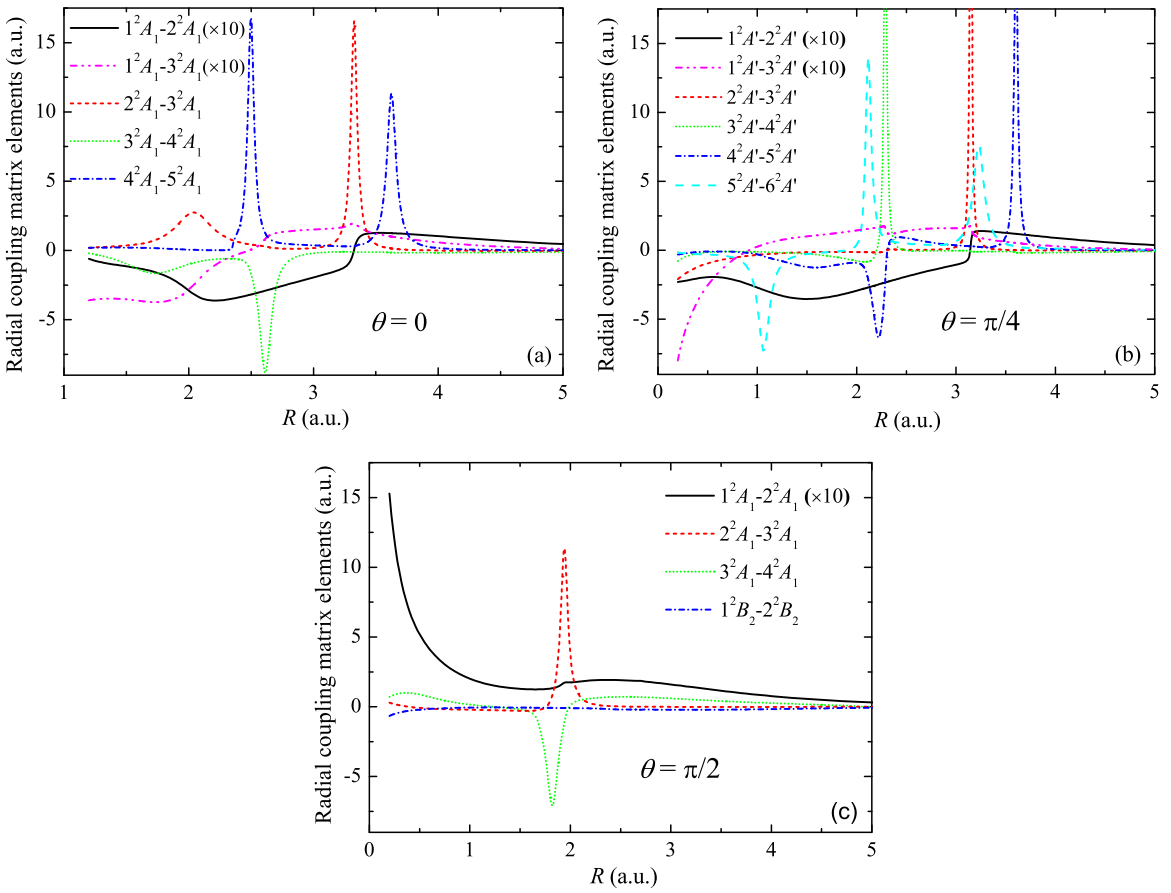

FIG. 4. (Color online) Radial coupling matrix elements for HeH_2^+. (a) $\theta = 0$; (b) $\theta = \pi/4$; (c) $\theta = \pi/2$.

R intervals 1.7–2.7 a.u. and 2.8–3.8 a.u. in Fig. 4), which promote the system to the upper states.

Figure 5(a) presents the rotational coupling matrix elements between the 1^2A_1 and 1^2B_1 states for $\theta = 0$ and $\pi/2$ orientations, and between the $1^2A'$-$1^2A''$ states for the $\theta = \pi/4$ orientation. For $R > 1.5$ a.u, the magnitudes of these matrix elements are similar for all three orientations. For $R < 1$ a.u., however, the rotational coupling for the $\theta = \pi/2$ orientation is significantly larger than for the other orientations. This means that it is easier to excite to the $H_2^+(2p\pi_u)$ + He state by rotational coupling for the perpendicular collision. The transition to the 1^2B_1 (or $1^2A''$) state will lead to dissociation of the H_2^+ molecule. For $\theta = 0$, the 1^2A_1-1^2B_2 rotational coupling has similar magnitude as the 1^2A_1-1^2B_1 coupling, and also induces the dissociation of H_2^+.

The rotational coupling matrix element between the states 1^2A_1 and 1^2B_2 [asymptotically converging to the $H_2^+(1s\sigma_g)$ + He and $H_2^+(2p\sigma_u)$ + He configurations] for

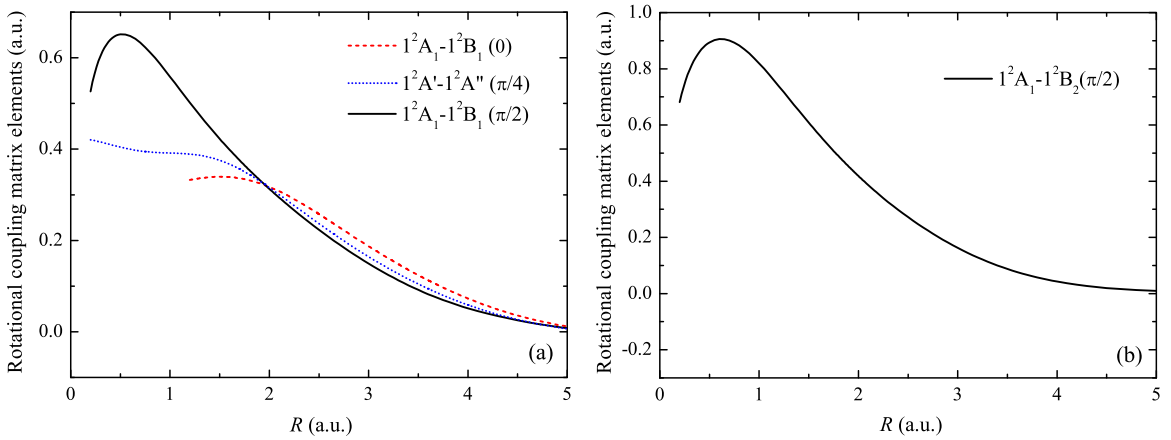

FIG. 5. (Color online) Rotational coupling matrix elements. (a) The 1^2A_1-1^2B_1 couplings for $\theta = 0$ and $\pi/2$, and the $1^2A'$-$1^2A''$ couplings for $\theta = \pi/4$; (b) the 1^2A_1-1^2B_2 coupling for $\theta = \pi/2$.

$\theta = \pi/2$ is shown in Fig. 5(b). From Fig. 3(c) we can see that the 1^2B_2 potential curve is very close to that of the 1^2A_1 state for $R < 1.5$ a.u. This induces a strong rotational coupling between them. This coupling will play the main role in the CID process [Eq. (1b)] for perpendicular collision. For $\theta = 0$, only radial couplings exist between the corresponding configurations.

In the C_s symmetry, because each A' state has both Σ and Π components, the rotational coupling matrix elements will have the Σ-Π and Π-Σ terms. In the QMOCC calculations, the rotational coupling matrix can be expressed as

$$P_{\alpha\beta} = \mp \frac{1}{2\mu R^2}[(J \mp \Lambda_\alpha)(J \pm \Lambda_\alpha + 1)]^{1/2} A^{\theta}_{\alpha\beta}\delta(\Lambda_\alpha, \Lambda_\beta \pm 1), \tag{4}$$

where μ is the reduced mass of the ion-atom pair, J is the total angular momentum quantum number, and Λ is the projection of the total electronic angular momentum along the internuclear axis. $\Lambda = 0$ and 1 for Σ and Π states, respectively. $A^{\theta}_{\alpha\beta} = \langle\alpha|\, iL_y \,|\beta\rangle$ is the rotational coupling matrix elements. Except at very low collision energies, the main partial waves J are far larger than Λ. Then for the same partial wave, the rotational coupling matrix elements for $\Sigma_\alpha - \Pi_\beta$ and $\Pi_\alpha - \Sigma_\beta$ terms should multiply a coefficient with the same numerical value but different phase, so it is necessary to distinguish the $\Sigma_\alpha - \Pi_\beta$ term from the $\Pi_\alpha - \Sigma_\beta$ term of the rotational coupling matrix elements.

By modifying the rotational coupling calculation program, we calculated the $\Sigma_\alpha - \Pi_\beta$ and $\Pi_\alpha - \Sigma_\beta$ terms of the rotational coupling matrix elements of the HeH_2^+ system for $\theta = \pi/4$. In Fig. 6 we show the rotational coupling matrix elements of the lowest three states, which have dominant roles for CID and EC processes. At $R > 3.15$ a.u., the $\Sigma_\alpha - \Pi_\beta$ term of the $1^2A' - 2^2A'$ coupling is almost zero because both the $1^2A'$ and $2^2A'$ states are mainly Σ states. At $R < 3.15$ a.u., the $2^2A'$ state rapidly becomes a Π state, and the numerical value of the $1^2A' - 2^2A'$ coupling sharply increases. At $R < 1.5$ a.u., the Σ projection of the $1^2A'$ state slowly decreases and the Π projection increases. Accordingly, the numerical value of the $\Sigma_\alpha - \Pi_\beta$ term of the $1^2A' - 2^2A'$ coupling slowly decreases. At $R > 3.15$ a.u., the $2^2A' - 3^2A'$ coupling has a negative value. At $R < 3.15$ a.u., the numerical value of the $\Sigma_\alpha - \Pi_\beta$ term of the $2^2A' - 3^2A'$ coupling rapidly decreased and the phase changed. This is because the main configurations of $2^2A'$ and $3^2A'$ states exchanged. The $2^2A'$ state from a main Σ state changed to a main Π state. At $R < 2.3$ a.u., the $2^2A' - 3^2A'$ coupling varies sharply because there exists a strong anticrossing between the $3^2A'$ and $4^2A'$ states.

The $1^2A' - 3^2A'$ and $1^2A' - 2^2A'$ couplings are responsible for the CID and EC processes at R greater than 3.15 a.u., respectively. But at smaller R, the $1^2A' - 2^2A'$ couplings play the main role for the CID process because of the strong radial $2^2A' - 3^2A'$ coupling at 3.15 a.u. It can be seen that the $1^2A' - 2^2A'$ coupling and 1^2A_1-1^2B_2 coupling of $\theta = \pi/2$ show an increasing trend with the increase of the collision angle θ at $R < 3$ a.u. This indicates that the perpendicular collision make the projectile dissociation easier.

IV. CROSS SECTION RESULTS AND DISCUSSION

With the help of the computed potential energy curves and coupling matrix elements discussed above, we calculated the CID, EC, and DC cross sections in the energy range of 0.02–10 keV/u. The vibrational and rotational motions of the incident molecule are neglected in the calculation. With respect to the vibrational motion the sudden approximation is reliable for energies above 10 eV/u, while with respect to the rotational motion it is valid for energies above ~0.1 eV/u. [7]. For $\theta = 0$, five $^2A_1$ states and one $^2B_1$ state have been included in the calculations. For $\theta = \pi/2$, four $^2A_1$ states, two $^2B_1$ states, and one $^2B_2$ state were included, while for $\theta = \pi/4$, the calculations included six $^2A'$ states and one $^2A''$ state.

A. Collision-induced dissociation by electronic excitation

The excitation mechanisms involved in the CID process include both electronic excitation to a repulsive state of H_2^+ [mainly to the $H_2^+(2p\sigma_u)$ state] and vibrational excitation to the continuum states of H_2^+. In the present calculations, only the electronic excitation mechanism is involved. As mentioned before both the $2p\sigma_u$ and $2p\pi_u$ states of H_2^+ are included in the expansion basis and contribute to the CID process. The CID cross sections calculated in the present work for different molecular alignments are shown in Fig. 7. They are compared with the experimental measurements of Williams and Dunbar

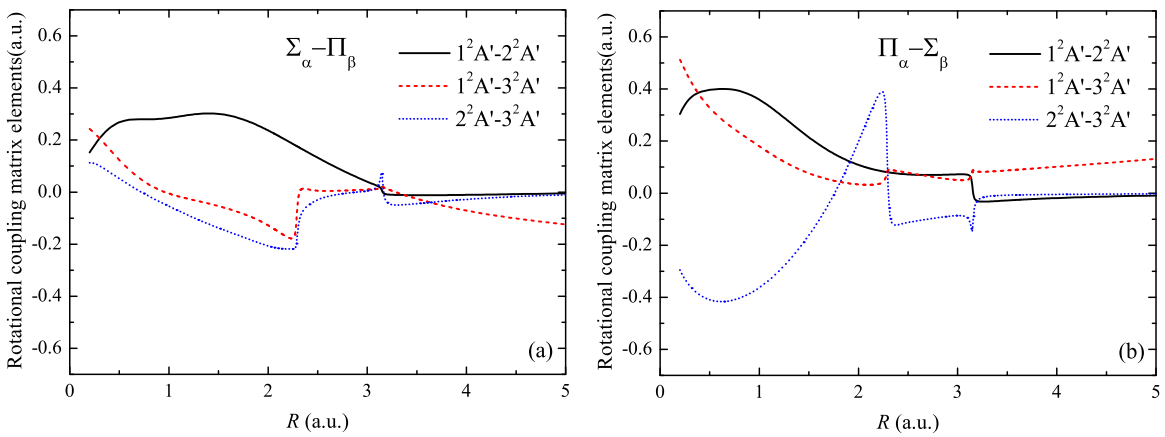

FIG. 6. (Color online) Rotational coupling matrix elements for $\theta = \pi/4$. (a) $\Sigma_\alpha - \Pi_\beta$; (b) $\Pi_\alpha - \Sigma_\beta$.

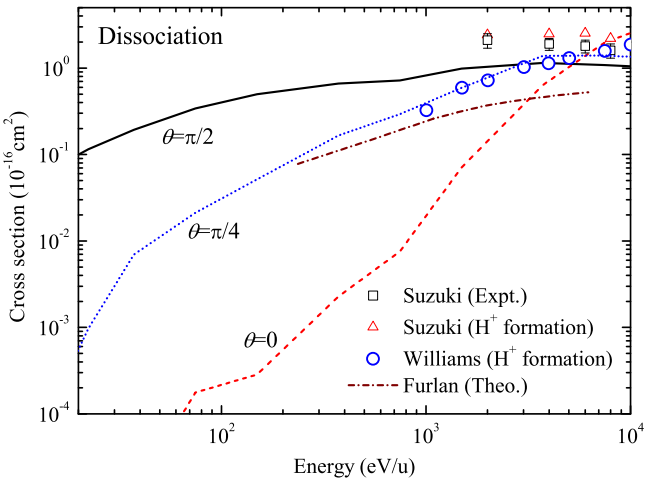

FIG. 7. (Color online) The CID cross sections for $H_2^+(2s) + He(1s^2)$ collision. The present results are compared with the experimental data of Suzuki *et al.* [1] and Williams and Dunbar [2], as well as the calculations of Furlan and Russek [10].

[2] and Suzuki *et al.* [3], as well as the theoretical results of Furlan and Russek [10]. Also shown in Fig. 7 are the H^+ formation results of Ref. [3]. The results of Ref. [2] are obtained by detection of the proton production, which would also include the ionization of H_2^+. The ionization process is expected to be considerably weak in the considered energy region, because it requires much larger excitation energy than the excitation of the H_2^+ to the $2p\sigma_u$ and $2p\pi_u$ states. The measurements of Suzuki *et al.* [3] show that the ionization process contributes no more than 20% to the H^+ production for H_2^+ energies in the range 4–16 keV. The experiment of Guidini [19] on H_2^+-H_2 collision also shows that the ionization cross sections are less than 5% of the total H^+ production for H_2^+ energies smaller than 15 keV.

The present results for the $\theta = \pi/4$ orientation, which should be close to the averaged result over all orientations, appear to merge well with the experimental results of Williams and Dunbar [2], while there is a serious discrepancy between our cross sections for any of the three orientations and the measurements of Suzuki *et al.* [3]. The present results show a monotonic increase of the CID cross section when the energy increases. In contrast, the cross sections of Suzuki *et al.* [3] show a slowly decreasing trend with increasing the energy, with a magnitude larger than the present calculations for any of the selected orientations and the experimental results of Ref. [2]. We note that in the experiment of Martinez and Yousif [20] on H_2^+-Ar collision, the energy dependence of the H^+ production cross section is also different than that of Suzuki *et al.* [3]. The magnitude of their result [20] is smaller than that in Ref. [3], and the discrepancy becomes larger with decreasing the energy.

Several reasons may contribute to the discrepancy between the experimental and theoretical results. The main reason may be the fact that the CID process is dependent on the initial vibrational state of the H_2^+ ion. In our calculations, only the ground vibrational state of H_2^+ was considered, while the experiments are usually performed with H_2^+ projectiles having a distribution of vibrational excited states. As Martinez and Yousif [20] have pointed out, the different population of these states in the ion source depends on the collisional history of the ions, and will result in disagreements between different experimental measurements. For collision energies of 1 keV, Lindsay *et al.* [21] have proved experimentally that the dissociation cross section from the $v = 5$ vibrational state is about two times larger than that from the ground vibrational state of H_2^+. This is a mere consequence of the fact that the vertical transition energy from the $v = 5$ vibrational level to the potential energy curve of the $2p\sigma_u$ state is significantly smaller than the one for transition from the $v = 0$ level.

Another possible reason for the discrepancy between present theoretical results and experimental data could be that, in the experiment, both the electronic excitation and the excitation to the vibrational continuum could contribute to the measured CID cross section. However, it was proven experimentally [20,22] that the dissociation process through excitation of the vibrational continuum is not important for energies above 0.2 keV/u, and the electronic CID is orders of magnitude larger than that of vibrational CID.

Furthermore, in the experiment contribution to the CID process may come not only from the excitation of $2p\sigma_u$ and $2p\pi_u$ states of H_2^+, but also from excitation of higher Rydberg states of H_2^+. However, the excitation of higher Rydberg states would require collision energies higher than those required for excitation of the $2p\sigma_u$ and $2p\pi_u$ states of H_2^+. Our calculations show that the contribution of the $2p\pi_u$ state gives less than 30% to the total CID cross section at 10 keV/u. With decreasing the energy, the contribution of the $2p\pi_u$ state slowly decreases. This indicates that the contribution to the CID process from the higher repulsive states of H_2^+, even when the corresponding energy thresholds are reached, would be much smaller than that coming from the excitation of the $2p\sigma_u$ state. However, the situation changes when H_2^+ is initially in a high vibrational state. The experimental study of the proton-production process in $H_2^+ + He$ collisions at 4 keV by Jaecks *et al.* [23] has shown that when H_2^+ is initially in a high vibrational state dominant contributions to the CID process come from the $1s\sigma_g \rightarrow 2p\pi_u$ and $1s\sigma_g \rightarrow 3d\sigma_g$ excitations.

In the theoretical work of Furlan and Russek [10], the calculations are limited to a three-state approximation, in which they include only the lowest three molecular states asymptotically converging to the $H_2^+(1s\sigma_g) + He$, $H_2(1s\,^1\Sigma g) + He^+$, and $H_2^+(2p\sigma_u) + He$ configurations. The results are obtained by averaging the calculated results for the 0, $\pi/6$, $\pi/3$, and $\pi/2$ orientations. Their CID cross section is several times smaller than the result of present calculations as well as the experimental results [2,3]. They attribute the discrepancy with the experimental measurements to the process of polarization-induced vibrational dissociation, pointing out that this process should contribute considerably to the experimental dissociation results. But as we have mentioned previously, the vibrational dissociation is not expected to be important in the keV region [20,22]. Using the same three-state approximation, we did the calculation and obtained CID cross sections similar to the present multistate results in the considered energy region. Therefore, the observed discrepancy has to be a result of some numerical problems in the calculations of Ref. [10].

The CID cross sections are several times larger than those for the EC and DC processes (see Figs. 7–9). The

present calculations show that the dissociation process strongly depends on the molecular alignments. For energies above 5 keV/u, the CID results with different alignments differ weakly with each other. With the decrease of collision energy, the CID results decrease relatively slowly for perpendicular collision ($\theta = \pi/2$), but for the $\theta = 0$ geometry the CID cross section decreases rapidly in the considered energy range. As mentioned earlier, in the case of perpendicular collision, the rotational couplings play a dominant role in the CID process. The initial state 1^2A_1 is strongly rotationally coupled with the 1^2B_2 state [see Fig. 5(b)], which asymptotically correlates with the $H_2^+(2p\sigma_u)$ + He state and contributes to the CID process. There are two molecular states, 3^2A_1 and 1^2B_1, that asymptotically correlate to the $H_2^+(2p\pi_u)$ + He state, which also contributes to CID. The initial state is weakly radially coupled with the 2^2A_1 state at small internuclear distance; the latter, however, is strongly radially coupled with the 3^2A_1 state at about 2 a.u. [cf. Fig. 4(c)] and will populate the 3^2A_1 state in the receding stage of the collision. The 1^2B_1 state is rotationally coupled directly with the initial state [cf. Fig. 5(a)], and contributes to the population of the $2p\pi_u$ state. In the $\theta = 0$ collision geometry, the initial state can be coupled with the 3^2A_1 state only indirectly by radial couplings, which weakly populate the $2p\sigma_u$ state. The 1^2B_1 state is weakly populated by the 1^2A_1-1^2B_1 rotational coupling. For collisions at $\theta = \pi/4$, both the radial and rotational couplings contribute to the excitation of the $2p\sigma_u$ state, and the cross section lies between the results for $\theta = 0$ and $\theta = \pi/2$ geometries.

B. Electron capture

In Fig. 8 we present the EC cross sections for the selected three collision geometries, corresponding to the $H_2(1s\ ^1\Sigma_g) + He^+$ exit channel. In the C_{2v} symmetry this asymptotic configuration correlates with the 2^2A_1 state, while in the C_s symmetry it correlates with $2^2A'$ state. Except for the perpendicular collision geometry, the initial state is weakly radially coupled with the 2^2A_1 or $2^2A'$ state at small R. However, the states 2^2A_1 and $2^2A'$ are strongly coupled, respectively, with the 3^2A_1 and $3^2A'$ states [that asymptotically correlate with the $H_2^+(2p\sigma_u)$ state] at about 3 a.u. The $2^2A_1 - 3^2A_1$ and $2^2A' - 3^2A'$ radial couplings at about 3 a.u. are very sharp and can be approximately treated as diabatic, so the $1^2A' - 2^2A'$ radial and rotational couplings at smaller R do not have apparent influence on the EC process, but mainly contribute to the CID process. The weak $1^2A' - 3^2A'$ (or 1^2A_1-2^2A_1 for $\theta = \pi/2$) radial couplings at $R < 3$ a.u. and other couplings with the $3^2A'$ state (or 2^2A_1 state for $\theta = \pi/2$) contribute to the EC process directly. The strong rotational couplings have no apparent influence on the EC process. The EC cross sections are, therefore, several times smaller than the CID cross section, and they weakly depend on the collision alignments. The EC cross sections exhibit some oscillation structures, especially pronounced for energies below ~1–2 keV/u. These structures are induced by the strong $2^2A_1 - 3^2A_1$ (or 3^2A_1-4^2A_1, $3^2A'$-$4^2A'$) radial coupling for $\theta = \pi/2$ (or $\theta = 0, \pi/4$) at about 2 a.u.

The EC result of Furlan and Russek [10], also shown in Fig. 8, is more than five times larger than the results of the present calculations as well as the experimental results of Ref. [3] (see Fig. 8). Using the same three-state approximation that was used in Ref. [10], we obtained the results which are a little larger (no more than three times for $E > 200$ eV/u) than the present results. The present EC results for any of the selected orientations are close to the experimental results of Suzuki *et al.* [3] in the overlapping energy region (above 2 keV/u). Below this energy, however, the present cross section for the $\theta = 0$ orientation decreases with decreasing the energy much faster than for the other two orientations.

C. Dissociative capture

In Fig. 9 we present the DC cross sections for the selected three orientations of the collision velocity vector. The DC process is related to the electron capture to the $H_2(2p\ ^3\Sigma_u)$ dissociating state. The present results are compared with the experimental measurements of Suzuki *et al.* [3]. Similarly as

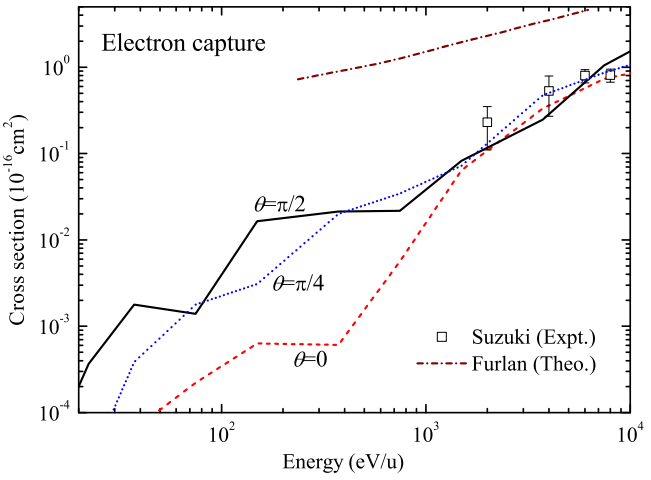

FIG. 8. (Color online) The EC cross sections for $H_2^+(2s) + He(1s^2)$ collision. The present results are compared with the calculations of Furlan and Russek [10] and the experimental measurements of Suzuki *et al.* [1]

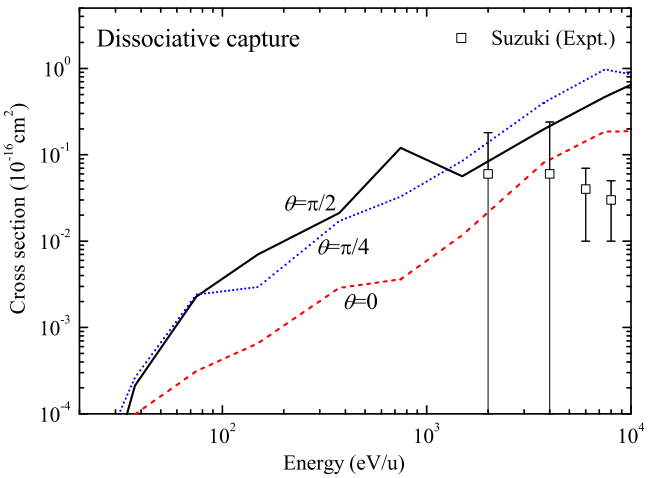

FIG. 9. (Color online) The DC cross sections for $H_2^+(2s)$ + $He(1s^2)$ collision. Experimental results are from Suzuki *et al.* [1].

in the case of the CID process, our DC cross sections decrease with decreasing the energy, while those of Ref. [3] have an opposite energy behavior. One should note, however, that very large uncertainties are associated with the experimental cross section values. It should be noted in Fig. 9 that the cross sections for the $\theta = \pi/2$ and $\theta = \pi/4$ orientations have similar magnitudes in the entire energy range considered, while the cross section for the $\theta = 0$ orientation is significantly smaller, but has a similar slope of decrease. Furhan and Russek [10] did not give the DC cross section because their three-state approximation did not include the corresponding configurations.

V. CONCLUSIONS

In the present work we have studied the CID, EC, and DC processes in $H_2^+ + He$ collisions using the QMOCC method in the energy range of 0.02–10 keV/u. The *ab initio* molecular structure data, used in the QMOCC calculations, were obtained by the MRDCI method for different orientations of the H_2^+ molecular axis with respect to the direction of collision velocity. Only the mechanism of electron excitation to a dissociative electronic state is included in the CID process in the present calculations. Our calculations show that the CID is the dominant process in this collision system, especially in the low-energy region. The rotational couplings play a very important role for the CID processes. The magnitude of the present averaged CID cross sections for different orientations is close to the experimental results of Williams and Dunbar [2], but is smaller than the measurements of Suzuki *et al.* [3]. The discrepancy is likely to be due to the fact that the initial vibrational state of the H_2^+ ions is different in different experiments and the theoretical calculations. The theoretical CID cross section of Furhan and Russek [10] by a three-state approximation is several times smaller than the present results and the experimental measurements, but their EC results are larger than the present calculations. The CID cross section sensitively depends on the molecular alignment, especially in the low-energy region. The dissociation is strongly favored when the molecular ion is aligned perpendicularly to the collision velocity direction. The dependence of the EC and DC cross sections on the orientation of the H_2^+ molecular axis with respect to the collision velocity vector is somewhat weaker than for the CID process.

ACKNOWLEDGMENTS

This work was supported by the National Basic Research Program of China (973 Program) (Grant No. 2013CB922200) and by the National Natural Science Foundation of China (Grants No. 11025417 and No. 11004014).

[1] N. V. Fedorenko, V. V. Afrosimov, R. N. Il'in, and D. M. Kaminker, Zh. Eksperim. Teor. Fiz. **36**, 385 (1959) [Sov. Phys. JETP **9**, 267 (1959)].
[2] J. F. Williams and D. N. F. Dunbar, Phys. Rev. **149**, 62 (1966).
[3] Y. Suzuki, T. Kaneko, and M. Tomita, J. Phys. Soc. Jpn. **55**, 3037 (1986).
[4] B. Van Zyl, D. Jaecks, D. Pretzer, and R. Geballe, Phys. Rev. **136**, A1561 (1964).
[5] G. H. Dunn, R. Geballe, and D. Pretzer, Phys. Rev. **128**, 2200 (1962).
[6] E. J. Quintana, A. Andriamasy, D. J. Schneider, and E. Pollack, Phys. Rev. A **39**, 5045 (1989).
[7] P. C. Stancil, Phys. Scr. T **110**, 340 (2004).
[8] V. Sidis, Adv. At. Mol. Phys. **26**, 161 (1990).
[9] T. A. Green and J. M. Peek, Phys. Rev. **169**, 37 (1968).
[10] R. J. Furlan and A. Russek, Phys. Rev. A **42**, 6436 (1990).
[11] B. H. Bransden and M. R. C. McDowell, in *Charge Exchange and the Theory of Ion-Atom Collisions* (Clarendon Press, Oxford, 1992).
[12] B. Zygelman, D. L. Cooper, M. J. Ford, A. Dalgarno, J. Gerratt, and M. Raimondi, Phys. Rev. A **46**, 3846 (1992).
[13] R. J. Buenker and R. A. Phillips, J. Mol. Struct.: THEOCHEM **123**, 291 (1985).
[14] S. Krebs and R. J. Buenker, J. Chem. Phys. **103**, 5613 (1995).
[15] L. F. Errea, J. D. Gorfinkiel, A. Macías, L. Méndez, and A. Riera, J. Phys. B **30**, 3855 (1997)
[16] B. R. Johnson, J. Comput. Phys. **13**, 445 (1973).
[17] M. C. Bacchus-Montabonel and P. Ceyzeriat, Phys. Rev. A **58**, 1162 (1998).
[18] T. H. Dunning, Jr., J. Chem. Phys. **90**, 1007 (1989).
[19] J. Guidini, C. R. Acad. Sci. (Paris) **253**, 829 (1961).
[20] H. Martínez and F. B. Yousif, Phys. Rev. A **69**, 062701 (2004).
[21] B. G. Lindsay, F. B. Yousif, and C. J. Latimer, J. Phys. B **21**, 2593 (1988).
[22] S. J. Anderson, J. Chem. Phys. **60**, 3278 (1974).
[23] D. H. Jaecks, O. Yenen, L. Wiese, and D. Calabrese, Phys. Rev. A **41**, 5934 (1990).